J. Fluid Mech. (2020), *vol.* 885, R2, doi:10.1017/jfm.2019.986

JFM RAPIDS
journals.cambridge.org/rapids

Scale separation and dependence of entrainment bubble-size distribution in free-surface turbulence

Xiangming Yu[1], **Kelli Hendrickson**[1] **and Dick K. P. Yue**[1,†]

[1]Department of Mechanical Engineering, Massachusetts Institute of Technology, Cambridge, MA 02139, USA

(Received 22 August 2019; revised 7 November 2019; accepted 14 November 2019)

We consider the size spectrum of entrained bubbles under strong free-surface turbulence (SFST). We investigate the entrainment bubble-size spectrum per unit (mean) interface area, $\mathcal{N}_a^E(r)$, with dimension length^{-3}, and develop a physical/mechanistic model for $\mathcal{N}_a^E(r)$ through energy arguments. The model obtains two distinct regimes of $\mathcal{N}_a^E(r)$, separated by bubble-size scale r_0. For bubble radius $r > r_0$, the effects of gravity g dominate those of the surface tension force σ/ρ, and $\mathcal{N}_a^E(r) \propto g^{-1}\epsilon^{2/3}r^{-10/3}$, where ϵ is the turbulence dissipation rate. For $r < r_0$, surface tension is more important and $\mathcal{N}_a^E(r) \propto (\sigma/\rho)^{-1}\epsilon^{2/3}r^{-4/3}$. From the model, we show that $r_0 \approx r_c = 1/2\sqrt{\sigma/\rho g}$, the capillary length scale, and not the generally assumed Hinze scale r_H. For an air–water interface and Earth gravity, $r_c \approx 1.5$ mm. The model provides an ϵ–r entrainment regime map that identifies a critical dissipation rate ϵ_{cr} (constant for given g and σ/ρ) above which there is appreciable air entrainment, thus separating SFST and weak FST. We confirm the theoretical model and its predictions using two-phase, high-fidelity direct numerical simulations of a canonical FST flow using the conservative volume-of-fluid method: the respective power laws of $\mathcal{N}_a^E(r) \propto r^{-10/3}$ and $r^{-4/3}$ for $r > r_0$ and $r < r_0$; the value $r_0 = r_c$; the scaling $\mathcal{N}_a^E(r) \propto \epsilon^{2/3}$; and the predictions of the ϵ–r entrainment regime map.

Key words: bubble dynamics, multiphase flow

1. Introduction

Air entrainment occurs and plays important roles in both natural processes and engineering applications. Quantifying the total volume, size distribution and scale dependence of entrained air in free-surface turbulence is key to modelling the natural air entrainment and gas transfer across the air–sea interface in ocean breaking waves

† Email address for correspondence: yue@mit.edu

(Deane & Stokes 2002) and the design of aeration cascades to increase oxygen concentration in water treatment plants (Chanson 1996).

To date, much of the understanding of air entrainment is in the context of breaking waves. Deane & Stokes (2002) measured the bulk bubble-size spectra (per unit volume) $N(r)$ inside breaking waves in the laboratory. In the initial acoustic phase, when entrainment primarily occurs, they identified two distinct power-law regimes of $N(r)$, depending on the bubble size r. For $r \gtrsim 1$ mm, $N(r) \propto r^{-10/3}$, while for $r \lesssim 1$ mm, $N(r) \propto r^{-3/2}$. They calculated the Hinze scale r_H (Hinze 1955) using

$$r_H = 2^{-8/5}(We_c\,\sigma/\rho)^{3/5}\epsilon^{-2/5}, \tag{1.1}$$

where $We_c \approx 4.7$ is the critical Weber number for bubble breakup by turbulence predicted from experiments (Lewis 1982; Martínez-Bazán, Montanes & Lasheras 1999). Using the fact that r_H in the experiments was close to the separation scale $r_0 \sim 1$ mm, they argued that r_0 is r_H. In the quiescent phase ($\sim$1.5 s after the acoustic phase) the bubble plume evolved rapidly under the influence of advection, turbulent diffusion and buoyant degassing, with an accompanying (more complex) evolution of $N(r)$. For the air entrainment phase, other researchers (Loewen, O'Dor & Skafel 1996; Rojas & Loewen 2007; Blenkinsopp & Chaplin 2010; Deike, Melville & Popinet 2016; Wang, Yang & Stern 2016) confirm the power-law dependence $N(r) \propto r^{-10/3}$ for larger bubbles in breaking waves experiments and simulations. For the regime $r \lesssim r_0$, Rojas & Loewen (2007) and Wang *et al.* (2016) obtained similar results to those of Deane & Stokes (2002).

Several parameterizations have been proposed for the air entrainment phase $N(r)$. Garrett, Li & Farmer (2000) performed a dimensional analysis in which $N(r)$ (dimension L^{-4}) is assumed to depend on the turbulence dissipation rate ϵ, the average rate of supply of air Q and the bubble radius r, and obtained a parameterization of the form

$$N(r) \propto Q\epsilon^{-1/3}r^{-10/3}. \tag{1.2}$$

Deane & Stokes (2002) pointed out that (1.2) is valid only for $r \gtrsim r_H$. For $r \lesssim r_H$, surface tension becomes important, requiring a different scale dependence. Performing a similar dimensional analysis for $r < r_H$, and assuming $N(r)$ is a multiplicative function of surface tension σ, liquid density ρ, jet velocity v and bubble radius r, they obtain a $N(r)$ scaling for these smaller bubbles:

$$N(r) \propto Q(\sigma/\rho)^{-3/2}v^2r^{-3/2}. \tag{1.3}$$

The models (1.2) and (1.3) originate from dimensional analysis and it is not clear if they reflect all of the underlying physical mechanism(s) of air entrainment. In particular, the inverse dependence on ϵ in (1.2) and the non-dependence on ϵ in (1.3) of $N(r)$ seem non-physical. Since turbulence provides energy for bubble entrainment (Brocchini & Peregrine 2001), a greater ϵ should increase the magnitude of $N(r)$. Deike *et al.* (2016) argued that Q should itself be a function of ϵ, and the combination of Q and $\epsilon^{-1/3}$ in (1.2) could lead to a positive exponent for ϵ. Similarly for (1.3), we can obtain a scaling of $\epsilon^{2/3}$ instead of ϵ^0 if $\epsilon \propto v^3/D_j$, with D_j the jet diameter. Finally, the identification of the regime separation scale r_0 with the Hinze scale r_H, while physically plausible, is not definitive. The possibility that r_0 derives from other relevant physical scales of the problem cannot be ruled out.

In this paper, we investigate the air entrainment across a free surface induced by underlying strong free-surface turbulence (SFST), specifically its bubble-size

distribution and scale dependence. We define $\mathcal{N}_a^E(r)$ (dimension L^{-3}) as the bubble-size spectrum per unit mean interface area (over a unit time in the quasi-steady air entrainment process). Through energy arguments, we show (in § 2) that $\mathcal{N}_a^E(r)$ follows two power-law regimes, depending on bubble size r, separated by a bubble-size length scale r_0. For $r > r_0$, $\mathcal{N}_a^E(r)$ scales as $g^{-1}\epsilon^{2/3}r^{-10/3}$, describing a gravity-dominated entrainment regime. For $r < r_0$, $\mathcal{N}_a^E(r)$ scales as $(\sigma/\rho)^{-1}\epsilon^{2/3}r^{-4/3}$, describing a surface-tension-dominated entrainment regime. We show that r_0 is in fact the capillary scale $r_c = 1/2\sqrt{\sigma/\rho g}$, independent of flow parameters such as ϵ; and hence not related to the Hinze scale r_H as is often assumed (Deane & Stokes 2002; Wang *et al.* 2016). Inspired by the diagram of the (L, q)-plane in Brocchini & Peregrine (2001), we derive a (r, ϵ)-plane prediction of when air entrainment occurs in free-surface turbulence (FST). The resulting regime map predicts a critical dissipation value ϵ_{cr} below which air entrainment is suppressed, thus demarcating weak FST (WFST) from SFST in terms of air entrainment. Like r_0, ϵ_{cr} depends only on the physical constants g and σ/ρ.

In § 3, we confirm our theoretical predictions using high-resolution direct numerical simulations (DNS) of canonical FST flows, solving three-dimensional two-phase incompressible Navier–Stokes equations with a fully nonlinear interface resolved by the conservative volume-of-fluid method (cVOF) (Weymouth & Yue 2010). We note that the surface entrainment size spectrum $\mathcal{N}_a^E(r)$ has a direct relationship to the (bulk) volume size spectrum $N_a(r)$ generally measured in experiments and simulations by labelling and sizing bubbles in the bulk. For a relatively short time after the onset of entrainment, before subsurface mechanisms come into play, $N_a(r)$ closely resembles $\mathcal{N}_a^E(r)$ in terms of the power-law regimes and slopes. With increasing time, $N_a(r)$ evolves (primarily) as a result of turbulent bubble fragmentation and degassing, and can become qualitatively different from $\mathcal{N}_a^E(r)$ (Yu *et al.* 2019). We perform DNS over a range of Froude (Fr) and Weber (We) numbers for the FST and obtain $N_a(r)$ at a relatively early time. The DNS confirms the key predictions of the scaling model: the gravity- and surface-tension-dominated power-law regimes and slopes; the separation scale $r_0 = r_c$ ($\approx$1.5 mm for an air–water interface in Earth gravity); and the scaling with $\epsilon^{2/3}$ (over the range we considered). Plotting the DNS data on the ϵ–r regime map also confirms the critical dissipation for air entrainment, $\epsilon_{cr} \sim O(10^{-2}\ \mathrm{m^2\ s^{-3}})$, for an air–water interface and Earth gravity.

2. Scaling for bubble-size distribution of air entrainment in SFST

To model the size spectrum of entrainment across a given free-surface area, we consider the entrainment size spectrum $\mathcal{N}_a^E(r)$, of dimension L^{-3}, where $\mathcal{N}_a^E(r')\delta r$ is the number of bubbles of (equivalent) radius $r' < r < r' + \delta r$ entrained per unit (mean) free-surface area. For simplicity, we assume quasi-steady air entrainment over unit time. A physical/mechanistic derivation for the scaling of $\mathcal{N}_a^E(r)$ through an energy argument requires two assumptions. First, we assume that the only source of bubble generation is the surrounding turbulence (Brocchini & Peregrine 2001). Second, we assume that the void fraction of bubbles is small and does not affect the dynamics of the bulk water turbulence (Garrett *et al.* 2000).

Consider a simplified entrainment scenario of a static spherical air bubble of radius r formed at a depth $2r\alpha$ under the free surface (a change in energy between Scenario 1 and 2 sketched in figure 1*a*). We assume the constant α is of order 1 to account for this simplification. The minimum energy required to entrain such a bubble, $E_b(r)$,

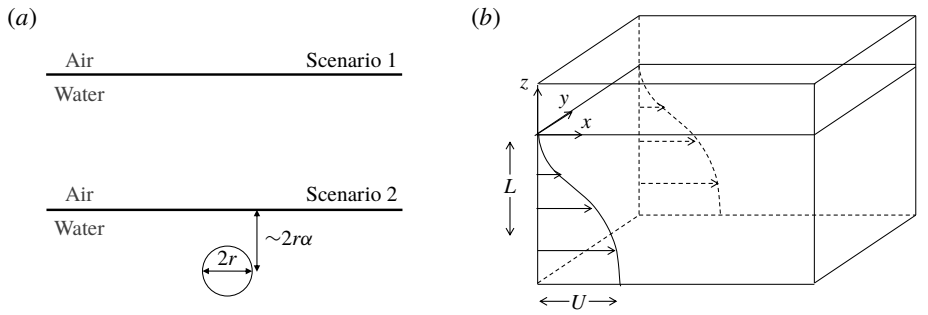

FIGURE 1. (*a*) Scenarios considered in the energy argument for bubble entrainment. (*b*) Sheared free-surface turbulent flow for DNS. Yu *et al.* (2019) contains full simulation details.

is the sum of the potential energy and the surface energy:

$$E_b(r) = g\frac{4}{3}\pi r^3 2r\alpha + \frac{\sigma}{\rho}4\pi r^2. \tag{2.1}$$

The total number of bubbles of radius r entrained across a (initial) surface area A_h is $\mathcal{N}_a^E(r)A_h\,\mathrm{d}r$ and the total energy required for entrainment of these bubbles is

$$\mathcal{N}_a^E(r)A_h\,\mathrm{d}rE_b(r) = \mathcal{N}_a^E(r)A_h\,\mathrm{d}r\left(g\frac{4}{3}\pi r^3 2r\alpha + \frac{\sigma}{\rho}4\pi r^2\right). \tag{2.2}$$

Using our first assumption, this amount of energy is supplied by turbulence over a near-surface region of depth r (around the entrained bubbles). Defining $E(k)$ as the turbulence energy spectrum, the turbulence energy per unit volume at length scale $1/k$ is given by $|E(k)\,\mathrm{d}k|$. We argue that the turbulence of length scale $1/k$ is primarily responsible for the entrainment of bubbles of radius $r \sim 1/k$. The available energy supplied by near-surface turbulence for entrainment within a volume $A_h r$ is proportional to

$$|E(k)\,\mathrm{d}k|A_h r \propto |E(r^{-1})\,\mathrm{d}r^{-1}|A_h r = E(r^{-1})r^{-2}\,\mathrm{d}rA_h r. \tag{2.3}$$

From an energy argument, (2.2) is proportional to (2.3) which yields

$$\mathcal{N}_a^E(r)A_h\,\mathrm{d}r\left(g\frac{4}{3}\pi r^3 2r\alpha + \frac{\sigma}{\rho}4\pi r^2\right) \propto E(r^{-1})r^{-2}\,\mathrm{d}rA_h r. \tag{2.4}$$

For SFST, the characteristic large surface deformations (and large Fr and We) weaken the free-surface boundary conditions, resulting in essentially isotropic near-surface turbulence (Yu *et al.* 2019). Thus, the Kolmogorov spectrum $E(r^{-1}) \propto \epsilon^{2/3}r^{5/3}$ provides the near-surface turbulence energy spectrum (this is also confirmed in the DNS, see figure 4). Using the Kolmogorov spectrum, (2.4) becomes

$$\mathcal{N}_a^E(r) \propto \left(\frac{2}{3}gr\alpha + \frac{\sigma}{\rho}\frac{1}{r}\right)^{-1}\epsilon^{2/3}r^{-7/3}. \tag{2.5}$$

For flows with different underlying turbulence spectra (for example, due to large bubble density, Alméras *et al.* 2017), the predicted bubble-size spectra will be modified accordingly.

From (2.5), we observe two regimes of entrainment by considering $f(r) = (2/3)gr\alpha + (\sigma/\rho)(1/r)$. For large r, gravity dominates $f(r)$ as $(2/3)gr\alpha$ is large, and (2.5) becomes

$$\mathcal{N}_a^E(r) \propto g^{-1}\epsilon^{2/3}r^{-10/3}. \tag{2.6}$$

For small r, surface tension dominates $f(r)$ as $(\sigma/\rho)(1/r)$ is large, and (2.5) becomes

$$\mathcal{N}_a^E(r) \propto (\sigma/\rho)^{-1}\epsilon^{2/3}r^{-4/3}. \tag{2.7}$$

The scale separating the two regimes r_0 occurs when the two terms in $f(r)$ are comparable at $r_0 = \sqrt{1.5\sigma/\alpha\rho g}$. This capillary scale $r_0 \approx r_c = 0.5\sqrt{\sigma/\rho g}$ corresponds to a balance between gravity and surface tension forces, or Bond number $Bo \equiv \rho g(2r_c)^2/\sigma = 1$.

We note that (2.6) and (2.7) are also obtained directly from dimensional analysis using the relevant set of physical parameters. In contrast to Garrett *et al.* (2000) and Deane & Stokes (2002), for free-surface air entrainment, the size spectrum per unit surface area, $\mathcal{N}_a^E(r)$ (dimension L^{-3}), is powered by the FST kinetic energy measured by ϵ (L^2T^{-3}). This is balanced by gravity g (LT^{-2}) and surface tension σ/ρ (L^3T^{-2}). Matching dimensions, we immediately obtain the scaling results for the respective size regimes.

Several remarks are in order. First, for the $r > r_0$ regime, the power-law slope $r^{-10/3}$ happens to coincide with that of Garrett *et al.* (2000) – for example, (1.2). However, the underlying physical processes in these two models are different in that Garrett *et al.* (2000) considered a cascade scenario of bubble fragmentation rather than air entrainment driven by surface turbulence as in our model. In fact, the slopes of the two power-law regimes in (2.6) and (2.7) result directly from the power-law slope of the near-surface isotropic SFST energy spectrum. One physical explanation for the coincidental similarity of the power-law slope of our model and Garrett *et al.* (2000) is to frame the air–water boundary of an initially large cavity immersed in an isotropic turbulent field as a free surface with underlying isotropic near-surface turbulence. In this context, the bubble generation process through fragmentation is similar to turbulence air entrainment (Hendrickson *et al.* 2019). Second, for $r < r_0$ in the surface-tension-dominated regime, the power-law slope in (2.7) differs (slightly) from the model of Deane & Stokes (2002) in (1.3). Third, the (positive exponent) dependence on turbulence dissipation rate $\sim\epsilon^{2/3}$ in the current models (2.6) and (2.7) is physically reasonable compared to that of (1.2) ($\sim\epsilon^{-1/3}$) and (1.3) ($\sim\epsilon^0$). In the current model, stronger surface turbulence leads to more entrainment. Finally, the separation scale r_0 is independent of flow parameters and not strictly related to the Hinze scale r_H as generally assumed (without strict theoretical consideration). The present theory provides a direct argument that r_0 is the physical capillary scale $r_0 \approx r_c$, which, for an air–water interface under the influence of Earth gravity, is $r_c \approx 1.5$ mm.

As discussed in § 1, the scale dependence of the surface entrainment size spectrum $\mathcal{N}_a^E(r)$ should be reflected in the underlying volume size spectrum $N_a(r)$ providing it is early enough in time, when fragmentation and degassing are not a factor. Figure 2 shows the theoretical prediction for $\mathcal{N}_a^E(r)$ in (2.5) superposed on available experimental and DNS data for $N_a(r)$ obtained for both breaking waves and SFST flows. For comparison of the spectral shape/slope, we normalize the magnitude of each dataset by its values at some (arbitrary) radius $r = 2$ mm. Despite the fact that

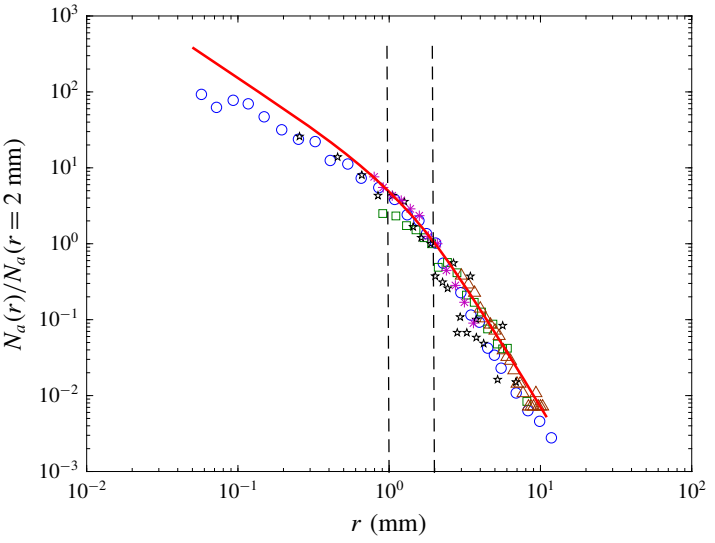

FIGURE 2. Comparison of $\mathcal{N}_a^E(r)$ in (2.5) (with $\alpha = 6$) and the measured bubble-size spectrum $N_a(r)$ inside breaking waves from the literature. All the data and (2.5) are normalized by their own values at $r = 2$ mm: ——, equation (2.5); ○, Deane & Stokes (2002); □, Rojas & Loewen (2007); ⋆, Wang *et al.* (2016); ∗, DNS of $Fr^2 = 21$, $We = 2100$ and $Re = 1200$ in § 3; △, Yu *et al.* (2019).

most of the datasets in figure 2 are from breaking waves, the scale dependence of the data appears to be well described by (2.5) for the entire range of r. We point out that in figure 2 the transition between the two regimes for most of the data occurs near $r_0 = 1$–2 mm, despite presumably different values of turbulent dissipation rates for the different datasets.

Air entrainment in SFST is a result of two competing effects on the free surface: the disrupting effect of near-surface turbulence and the stabilizing effect from gravity and surface tension. Comparing the two effects provides criteria for the lower and upper bounds r_l and r_u of bubble size that can be entrained. We argue that the lower bound r_l corresponds to a scale where turbulence disturbance is much smaller than surface tension forces – that is, $We_t = \rho\overline{v^2}(2r_l)/\sigma = We_l$ ($\ll 1$), where $\overline{v^2} \approx 2.0(\epsilon d)^{2/3}$ is the turbulence fluctuation over a distance $d = 2r_l$; r_l can be further written as

$$r_l = 2^{-8/5}(\sigma/\rho\, We_l)^{3/5}\epsilon^{-2/5}. \tag{2.8}$$

Equation (2.8) is the same form as the Hinze scale (1.1), with We_l replacing We_c. Both r_l and r_H correspond to the critical length scales resulting from the competition between near-surface turbulence and surface tension forces. While the length scale r_H is for bubbles with a stable spherical interface, r_l is the length scale associated with the breakup of a free surface with a relatively unstable flat interface. As such, we expect $We_l \ll We_c$ (and consequently $r_l \ll r_H$).

We define the upper bound bubble length scale r_u similarly from the (turbulence) Froude number $Fr_t^2 = \overline{v^2}/g(2r_u) = Fr_u^2$ ($\ll 1$), which yields

$$r_u = 4(Fr_u^2 g)^{-3}\epsilon^2. \tag{2.9}$$

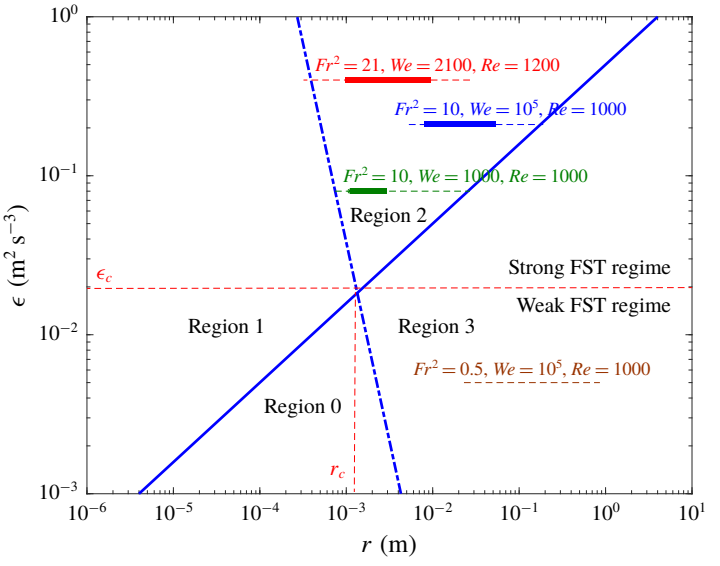

FIGURE 3. Conceptual ϵ–r regime map to predict FST-driven entrainment for an air–water interface under Earth gravity: -------- r_l of (2.8); —— r_u of (2.9); with $\epsilon_c \approx 0.02$ m^2 s^{-3} and $r_c \approx 1.5$ mm. For DNS data: ▬, range of measured entrained bubbles; - - -, potential size range of DNS. For visualization: $We_l \equiv 0.1$ and $Fr_u^2 \equiv 0.1$ (consistent with physical arguments).

With the expressions (2.8) and (2.9) in terms of ϵ, we obtain a critical turbulent dissipation ϵ_{cr} when $r_u(\epsilon_{cr}) = r_l(\epsilon_{cr})$, below which no entrainment would occur:

$$\epsilon_{cr} = C_\epsilon g^{5/4}(\sigma/\rho)^{1/4}. \tag{2.10}$$

As with the separation scale r_0 for $\mathcal{N}_a^E(r)$, ϵ_{cr} is a constant that depends only on the interface media and value of gravity. The upper and lower bounds (2.8) and (2.9) enable us to predict an ϵ–r regime map for bubble entrainment in FST (see figure 3, also see Brocchini & Peregrine (2001)). The dependencies of r_l and r_u on ϵ demarcate four regions in the (ϵ–r)-plane. The strong free-surface turbulence regime ($\epsilon > \epsilon_{cr}$) is where entrainment occurs within the size range $r_l < r < r_u$, which we denote Region 2 in figure 3. The bubble-size range increases with ϵ. Turbulence will not entrain bubbles outside of this size range due to dominant gravity or surface tension forces. The weak free-surface turbulence regime ($\epsilon < \epsilon_{cr}$) is where no entrainment occurs for three different physical reasons. In Region 1, $r < r_l$ and surface tension forces stabilize the free surface. In Region 3, $r > r_u$ and strong gravity forces suppress air entrainment. In Region 0, both gravity and surface tension forces suppress entrainment.

3. Direct numerical simulations of FST

We perform DNS of a canonical problem of three-dimensional incompressible two-phase (air and water) viscous turbulent flow with turbulent kinetic energy supplied by a sheared underlying bulk water flow (see figure 1*b*). Extensive documentation of the turbulence characteristics of this flow exists for non-entraining WFST at low Fr (Shen *et al.* 1999; Shen, Triantafyllou & Yue 2000, 2001; Shen & Yue 2001)

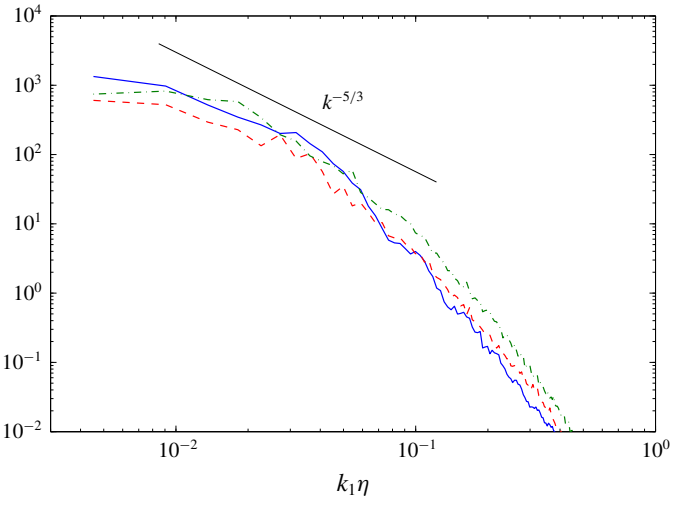

FIGURE 4. One-dimensional near-surface energy spectrum $E_{11}(k_1)$ (——), $E_{22}(k_1)$ (– – –), $E_{33}(k_1)$ (— · —) at $t = 56$ for DNS-1.

and air-entraining SFST at high Fr (Yu *et al.* 2019). We solve the three-dimensional two-phase incompressible Navier–Stokes equations with a fully nonlinear interface resolved by the cVOF method (Weymouth & Yue 2010), which conserves volume to machine accuracy. Yu *et al.* (2019) provides the details of numerical implementations and verifications. For the data presented here, the mean shear-flow depth L and velocity deficit U are the characteristic length and velocity scales and normalize all the variables unless otherwise stated, with $Fr^2 = U^2/gL$, $We = \rho U^2 L/\sigma$ and $Re = UL/\nu$. The domain size is 6^3 and the grid size $\Delta \approx 0.01$. In the analyses below, we report (only) bubbles that are considered resolved in the presence of surface tension in the DNS corresponding to equivalent diameter $2r \gtrsim 7\Delta$. The unreported entrained volume is $\lesssim 1\,\%$ for all cases. For SFST, we present results for two high-resolution DNS, both with $Bo = \rho g L^2/\sigma = 100$. DNS-1 has parameters $Fr^2 = 21$, $We = 2100$ and $Re = 1200$ and DNS-2 has $Fr^2 = 24.64$, $We = 2464$ and $Re = 1300$. We note that for constant g, σ/ρ and ν, DNS-2 has a larger U and the same L as DNS-1.

The DNS results capture the evolution of air-entraining SFST corresponding to large Fr and We (Yu *et al.* 2019). Briefly, starting from a quiescent free surface, the FST grows rapidly due to production by the bulk flow mean shear, followed by a quasi-steady active entrainment SFST period, after which the FST eventually decays (and entrainment ceases) due to turbulence diffusion and dissipation. We report results within the quasi-steady active entrainment SFST period. In this period, turbulence forms vortical structures of different length scales near the free surface and entrains bubbles of different sizes (Yu *et al.* 2019). Figure 4 shows the one-dimensional energy spectra of near-surface turbulence during the SFST period for DNS-1 (DNS-2 is similar). Consistent with the assumption in § 2, the turbulence shows isotropy, with the three components having comparable magnitudes and following the Kolmogorov $k^{-5/3}$ spectral slope.

Figure 5 shows the volume bubble-size spectra $N_a(r)$ for DNS-1 during the active entrainment period (r is normalized by the capillary scale r_c for clarity). The measured bulk spectrum provides direct support of the scale dependencies of (2.6) and (2.7),

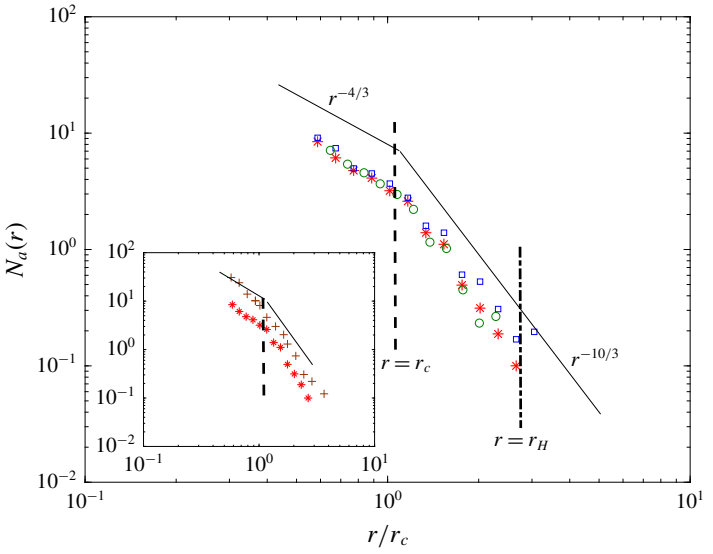

FIGURE 5. Volume bubble-size spectrum $N_a(r)$ during the active entrainment period of DNS-1: ○, at a time sampled within the entrainment period; □, at a time sampled close to the end of entrainment period; ∗, average of $N_a(r)$ at every $tL/U = 0.5$ within the entrainment period. Here $r_c = 0.5\sqrt{\sigma/\rho g}$ is the capillary length scale and r_H is the Hinze scale in (1.1). The two theoretical power laws of $r^{-4/3}$ and $r^{-10/3}$ are represented by ——. The inset shows the average volume bubble-size spectrum $N_a(r)$ (within the entrainment period) for: ∗, DNS-1; +, DNS-2.

respectively, for $r > r_0$ and $r < r_0$ with the separation scale $r_0 \approx r_c$. We estimate r_H (shown in figure 5) using the dimensionless form of (1.1), $r_H = 2^{-8/5}(We_c/We)^{3/5}\epsilon^{-2/5}$, using the DNS-1 near-surface turbulence dissipation rate $\epsilon \sim O(10^{-3})$ and $We_c = 4.7$. For DNS-1, r_H is approximately three times greater than r_c, and this scale separation allows us to confirm that the separation scale between the two regimes is indeed $r_0 \approx r_c$ and not r_H. For this particular DNS case, turbulence fragmentation of entrained bubbles should not have significant effects on $N_a(r)$ within the entrainment period, because r_H is at the upper bound of the measured entrainment. We confirm this by comparing the three spectra at different times for $r < r_H$ in figure 5. This enables us to estimate $\mathcal{N}_a^E(r)$ using $N_a(r)$ with confidence. The inset of figure 5 shows $N_a(r)$ for both DNS-1 and DNS-2 averaged over the entrainment period. For DNS-2, ϵ is increased by a factor of 1.5. However, r_0 is the same for both DNS datasets and occurs at r_c (which is the same for both DNS). This further confirms that r_0 between the two power-law entrainment regimes is in fact the capillary scale r_c and not the Hinze scale r_H, which changes with ϵ.

To confirm the scaling of the entrainment model with turbulent dissipation, we perform a series of lower-resolution DNS with $\Delta = 0.027$ for FST with $Fr^2 = 10$, $We = 50\,000$ and $Re = 1000$, varying the slope of the initial mean shear profile to achieve different values for ϵ. Figure 6 shows the linear dependence of the integral of averaged $N_a(r)$ (or entrained volume) plotted against $\overline{\epsilon^{2/3}}$ (averaged during the entrainment period), which confirms the positive exponent scaling of $\mathcal{N}_a^E(r) \propto \epsilon^{2/3}$ in (2.5). Linear regression obtains a horizontal intercept corresponding to $\overline{\epsilon^{2/3}} \approx 0.002$. When scaled by an air–water interface under Earth gravity, it provides an independent

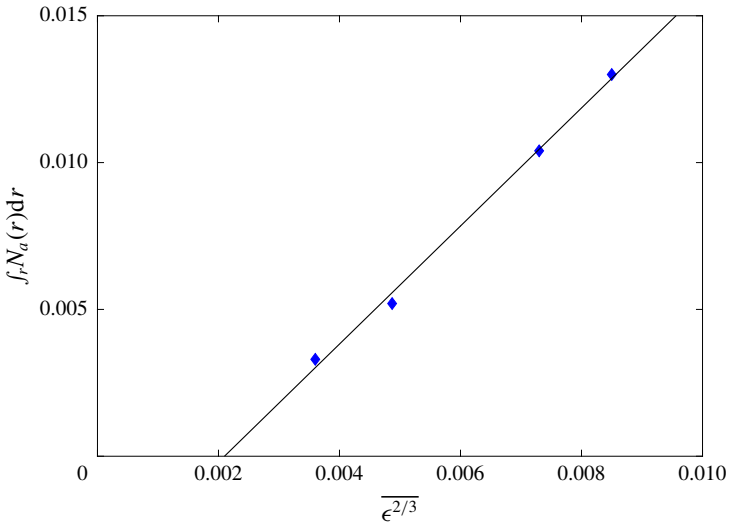

FIGURE 6. Integral of $N_a(r)$ over the resolved range of r plotted against $\overline{\epsilon^{2/3}}$, normalized by L and U (◆). The average is during the entrainment period for DNS with $Fr^2 = 10$ and $We = 50\,000$ and four variable shear profiles. ——: linear regression model $y = 2.01x - 0.00422$ with R-square 0.996.

estimate of $\epsilon_{cr} \approx 0.03$ m^2 s^{-3} that compares well to the 0.02 m^2 s^{-3} value obtained from figure 3.

Finally, we confirm the prediction of the ϵ–r entrainment regime map, figure 3, using FST DNS over a broad range of Fr^2, We and ϵ (by varying the initial mean shear profiles). We estimate the physical units of the characteristic length scale L and near-surface turbulence dissipation rate ϵ using the defined values of Fr^2, We and Re (and assume Earth gravity and an air–water interface). The measured size range of entrainment as functions of ϵ for the different cases are superimposed onto the map in figure 3 (heavy lines). Notice that r_l and r_u in (2.8) and (2.9) assume an unbounded turbulence inertial range. For each DNS case, the range of the entrainment bubble size has a lower bound of Δ and an upper bound of L as well. This range of (Δ, L) is represented by dashed lines. The selected DNS cases with/without air entrainment correctly fall into the predicted regions of strong/weak FST, substantially confirming the predictions of § 2.

4. Conclusion

We perform theoretical and numerical investigations of air entrainment, and specifically the entrainment bubble-size distribution under SFST. Using arguments relating the energy required for bubble entrainment/formation and available turbulent kinetic energy in the SFST, we obtain a theoretical model for the surface entrainment bubble-size spectrum $\mathcal{N}_a^E(r)$. The model describes two size regimes separated by a scale r_0, with $\mathcal{N}_a^E(r) \propto g^{-1}\epsilon^{2/3}r^{-10/3}$ for $r > r_0$, and $\mathcal{N}_a^E(r) \propto (\sigma/\rho)^{-1}\epsilon^{2/3}r^{-4/3}$ for $r < r_0$, where r is the (equivalent) bubble radius, g is gravity, σ is the surface tension, ρ is the water density and ϵ is the turbulent dissipation rate of the SFST. From the model, we obtain that r_0 is the capillary scale r_c (≈1.5 mm for an air–water interface under Earth gravity), distinct from the Hinze scale r_H. We also propose an

ϵ–r regime map to describe air entrainment in free-surface turbulent flows. The map predicts a critical value of the dissipation rate $\epsilon_{cr} \approx 0.02$ m^2 s^{-3} above which air entrainment occurs. High-resolution volume-conserving two-phase DNS of canonical shear-flow FST confirm the theoretical model and predictions. Namely, it provides direct evidence of the two power-law regimes and slopes, the separation scale $r_0 \approx r_c$, the positive exponent of the turbulent dissipation $\epsilon^{2/3}$, and the ϵ–r entrainment regime.

We remark that, while the (shear-flow) FST we consider is canonical and has been studied extensively theoretically and computationally, there exist few detailed experimental investigations of SFST air entrainment. Direct experimental measurements to support the present theoretical and DNS results would be invaluable. In particular, it would be useful to confirm the scale separation we find for additional combinations of ρ, σ and ϵ. The energy argument and predictions for SFST air entrainment may provide insights into more complex air-entraining, free-surface problems, such as wave breaking (see figure 2) and ship wakes (Hendrickson *et al.* 2019). These are subjects of our current investigations.

Acknowledgements

This work was funded by the Office of Naval Research N00014-10-1-0630 and N00014-17-1-2089 under the guidance of Dr K.-H. Kim and Dr T. C. Fu. The computational resources for the effort were funded through the High Performance Modernization Program at the Department of Defense.

Declaration of interests

The authors report no conflict of interest.

References

ALMÉRAS, E., MATHAI, V., LOHSE, D. & SUN, C. 2017 Experimental investigation of the turbulence induced by a bubble swarm rising within incident turbulence. *J. Fluid Mech.* **825**, 1091–1112.

BLENKINSOPP, C. E. & CHAPLIN, J. R. 2010 Bubble size measurements in breaking waves using optical fiber phase detection probes. *IEEE J. Ocean. Engng* **35** (2), 388–401.

BROCCHINI, M. & PEREGRINE, D. H. 2001 The dynamics of strong turbulence at free surfaces. Part 1. Description. *J. Fluid Mech.* **449**, 225–254.

CHANSON, H. 1996 *Air Bubble Entrainment in Free-surface Turbulent Shear Flows*. Elsevier.

DEANE, G. B. & STOKES, M. D. 2002 Scale dependence of bubble creation mechanisms in breaking waves. *Nature* **418** (6900), 839–844.

DEIKE, L., MELVILLE, W. K. & POPINET, S. 2016 Air entrainment and bubble statistics in breaking waves. *J. Fluid Mech.* **801**, 91–129.

GARRETT, C., LI, M. & FARMER, D. 2000 The connection between bubble size spectra and energy dissipation rates in the upper ocean. *J. Phys. Oceanogr.* **30** (9), 2163–2171.

HENDRICKSON, K., WEYMOUTH, G. D., YU, X. & YUE, D. K. P. 2019 Wake behind a three-dimensional dry transom stern. Part 1. Flow structure and large-scale air entrainment. *J. Fluid Mech.* **875**, 854–883.

HINZE, J. O. 1955 Fundamentals of the hydrodynamic mechanism of splitting in dispersion processes. *AIChE J.* **1** (3), 289–295.

LEWIS, D. A. 1982 Bubble splitting in shear flow. *Trans. Inst. Chem. Engrs* **60**, 283–291.

LOEWEN, M. R., O'DOR, M. A. & SKAFEL, M. G. 1996 Bubbles entrained by mechanically generated breaking waves. *J. Geophys. Res.* **101** (C9), 20759–20769.

MARTÍNEZ-BAZÁN, C., MONTANES, J. L. & LASHERAS, J. C. 1999 On the breakup of an air bubble injected into a fully developed turbulent flow. Part 1. Breakup frequency. *J. Fluid Mech.* **401**, 157–182.

ROJAS, G. & LOEWEN, M. R. 2007 Fiber-optic probe measurements of void fraction and bubble size distributions beneath breaking waves. *Exp. Fluids* **43** (6), 895–906.

SHEN, L., TRIANTAFYLLOU, G. S. & YUE, D. K. P. 2000 Turbulent diffusion near a free surface. *J. Fluid Mech.* **407**, 145–166.

SHEN, L., TRIANTAFYLLOU, G. S. & YUE, D. K. P. 2001 Mixing of a passive scalar near a free surface. *Phys. Fluids* **13** (4), 913–926.

SHEN, L. & YUE, D. K. P. 2001 Large-eddy simulation of free-surface turbulence. *J. Fluid Mech.* **440**, 75–116.

SHEN, L., ZHANG, X., YUE, D. K. P. & TRIANTAFYLLOU, G. S. 1999 The surface layer for free-surface turbulent flows. *J. Fluid Mech.* **386**, 167–212.

WANG, Z., YANG, J. & STERN, F. 2016 High-fidelity simulations of bubble, droplet and spray formation in breaking waves. *J. Fluid Mech.* **792**, 307–327.

WEYMOUTH, G. D. & YUE, D. K. P. 2010 Conservative volume-of-fluid method for free-surface simulations on Cartesian-grids. *J. Comput. Phys.* **229** (8), 2853–2865.

YU, X., HENDRICKSON, K., CAMPBELL, B. K. & YUE, D. K. P. 2019 Numerical investigation of shear-flow free-surface turbulence and air entrainment at large Froude and Weber numbers. *J. Fluid Mech.* **880**, 209–238.